Article

Alumina−Hydroxyapatite Millimetric Spheres for Cadmium(II) Removal in Aqueous Medium

Pamela Nair Silva-Holguín, Nahum A. Medellín-Castillo, E. Armando Zaragoza-Contreras, and Simón Yobanny Reyes-López*
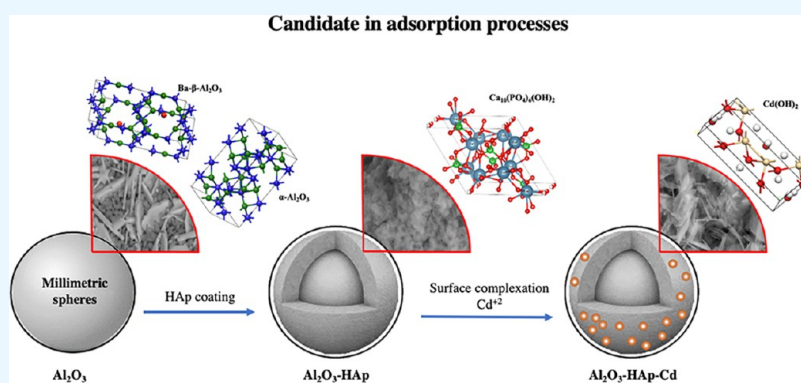
Read Online

ACCESS | Metrics & More | Article Recommendations

ABSTRACT: Heavy metals can act as selective agents in the development and proliferation of antibiotic-resistant bacteria through a process called coselection. In the year 2050, an estimated 10 million deaths will be caused by antibiotic-resistant bacteria; therefore, the presence of heavy metals in bodies of water represents an environmental and sanitary threat that requires efficient treatment processes and/or materials for their removal. In the present study, the effect of the hydroxyapatite coating on the adsorbent capacity of cadmium in alumina spheres was evaluated. The hydroxyapatite coating on the alumina sphere increased the surface area from 0.66 to 0.96 m^2/g and the number of acid sites from 0.064 to 0.306 meq/g and displaced the IEP of hydroxyapatite from 5.37 to 4.2, increasing the Cd^{2+} adsorbing capacity from 59.87 mg/g to 89.37 mg/g and promoting adsorption by surface complexation. Alumina-hydroxyapatite spheres stand out for their improved adsorbent properties and easy handling, which positioned this material as a potential alternative in adsorption processes.

INTRODUCTION

The presence of heavy metals in bodies of water represent a threat to all living organisms due to their high toxicity, nonbiodegradable properties, and bioaccumulation.[1] However, the toxicity of heavy metals is not a unique problem; in recent years, it has been observed that the development of antibiotic-resistant bacteria is not exclusively due to the presence of antibiotics but is also associated with the presence of heavy metals. Heavy metals can induce selective pressure on microbial populations leading to antimicrobial resistance through a mechanism called coselection.[2]

Heavy metal pollution in the environment is of particular interest as anthropogenic levels of heavy metals are several orders of magnitude higher than those of antibiotics; furthermore, unlike antibiotics, metals are not subject to degradation and thus persist in the environment.[3,4] The elevated and growing incidence of diseases caused by antibiotic-resistant bacteria represents a global problem;

projections for the year 2050 estimated 10 million deaths per year due to antibiotic resistance.[5]

Avoiding the release of heavy metals into the environment is an environmental and health issue that requires efficient treatment processes and materials for their removal in trace concentrations. This implies the development of effective, economical, sustainable remediation methods with low or no secondary contamination.[6] The adsorption process plays a fundamental role in the removal of trace contaminants in bodies of water because it is an economical, simple, easy-to-apply, and highly efficient process.[7] To consider an adsorbent material as an industrial candidate, certain properties must be

Table 1. Kinetic Models of Adsorption, Equation, and Parameters

model	equation	parameters
pseudo first order	$q_t = q_e(1 - e^{-(k_1 t)})$	q_t = adsorption capacity at time t (mg/g)
pseudo second order	$q_t = \dfrac{k_2 q_e^2 t}{1 + k_2 q_e t}$	q_e = adsorption capacity at equilibrium (mg/g)
		K_1 = first-order rate constant (min^{-1})
Elovich	$q_t = \beta \ln(\alpha \beta t)$	K_2 = second-order rate constant (g mg^{-1} h^{-1})
intraparticle diffusion	$q_t = K_{DI} t^{1/2}$	α = initial adsorption rate (mg g^{-1} min^{-1})
		β = desorption constant (g mg^{-1})
		K_{DI} = intraparticle diffusion rate constant (mg/g/min)

Table 2. Adsorption Equilibrium Models, Equation, and Parameters

model	equation	parameters
Langmuir	$q_e = \dfrac{q_m b C_e}{1 + b C_e}$	C_e = equilibrium concentration in liquid phase (mg/L)
		q_m = monolayer adsorption capacity (mg/g)
Freundlich	$q_e = K_F C_e^{\frac{1}{n}}$	b = Langmuir constant (L/mg)
		K_F = Freundlich constant (mg/g)
Temkin	$q_e = \dfrac{RT}{b_T} \ln(K_T C_e)$	$1/n$ = intensity of the adsorption
		B_T = constant related to adsorption temperature (L/g)
		K_T = Temkin constant
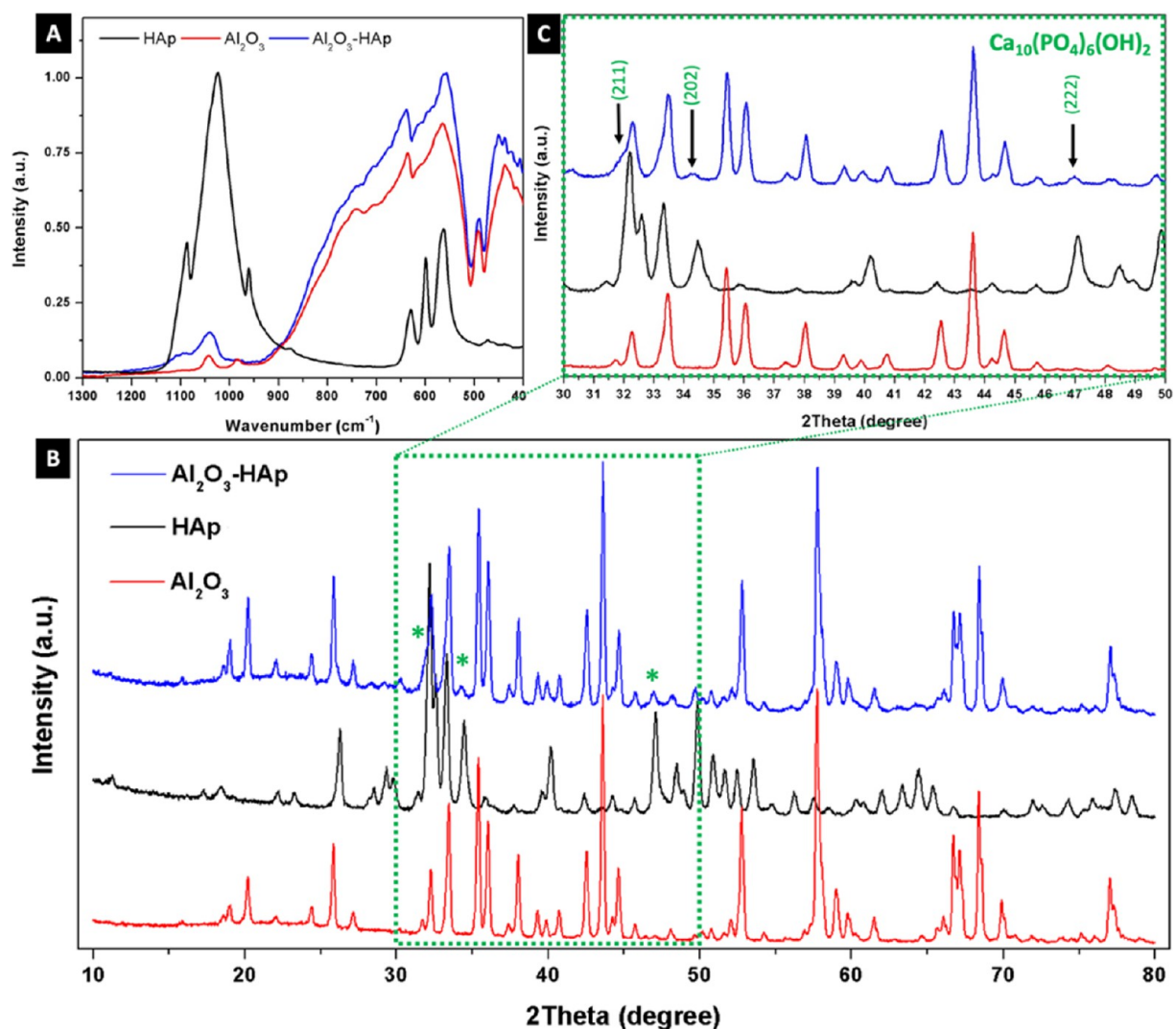
Figure 1. Al_2O_3−HAp spheres: (A) infrared spectrum of HAp, Al_2O_3, and Al_2O_3−HAp. (B) X-ray diffractogram of HAp, Al_2O_3, and Al_2O_3−HAp. (C) Enlargement of the green zone.
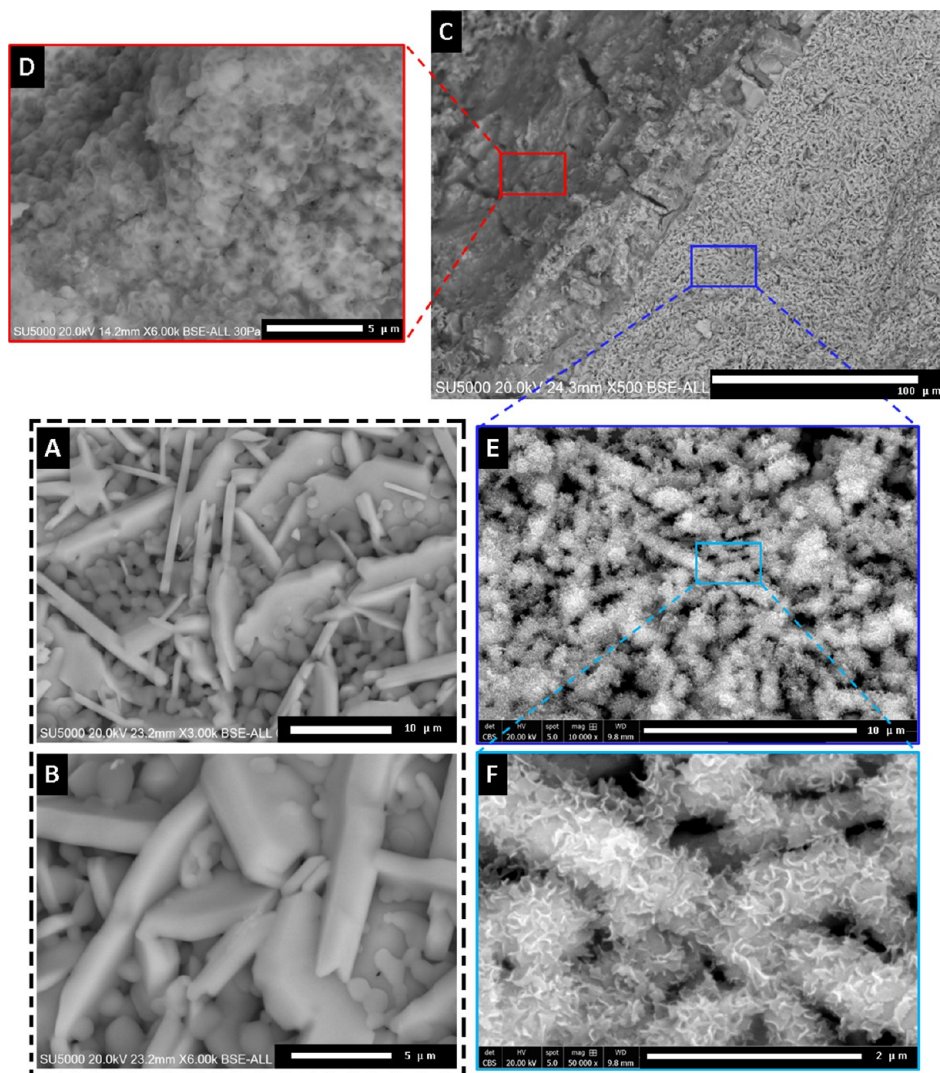
Figure 2. SEM micrographs of (A, B) surface Al_2O_3 spheres. (C) Cross section of Al_2O_3-HAp spheres. (D) Surface of Al_2O_3-HAp spheres. (E, F) Inside of Al_2O_3-HAp spheres.

met: competitive adsorbent capacity, strong adsorbent—adsorbate affinity, high surface area, high density of active sites, chemical stability under adverse environmental conditions, easy regeneration, and/or recovery after use.[6] The physicochemical properties of the surface of the material, like the specific surface area, the zeta potential (pZ), and the functional groups of the surface play a critical role in the adsorption capacity of metals.[8] Among adsorbent materials, ceramic materials are very attractive for adsorption processes because they present chemical stability in hostile mediums, porosity, and biocompatibility and are friendly to the environment.[9]

Alumina (Al_2O_3) is an aluminum oxide ceramic that presents various characteristics depending on the metastable (γ-, δ-, θ-, ι-, σ-, κ-, y-, η-Al_2O_3) or stable (α-Al_2O_3) phase in which it is found.[10] The γ-Al_2O_3 phase is the most used in adsorption processes, either in its pure form[11] or in combination with other adsorbent materials such as multi-walled carbon nanotubes.[12] The β-Al_2O_3 phase has also been studied for the adsorption of cadmium in aqueous medium.[13] Hydroxyapatite (HAp, $Ca_{10}(PO_4)_6(HO)_2$) is a biogenic calcium phosphate ceramic that presents biocompatibility[14] and easy availability from natural sources[7] or various synthesis

methods;[15] it is widely used in processes for the removal of various contaminants, among which heavy metals stand out, where adsorbent capacities have been obtained above 1300 mg/g.[16] However, one of the limitations of various adsorbent materials is their use in the form of powder or nanoparticles without a support matrix, which have high surface areas, but it is necessary to use additional techniques for their recovery after the adsorption process, which increases costs. Therefore, it is necessary to produce adsorbent materials that are easy to handle and recover and to know their physicochemical properties, as they have a certain shape and size, which facilitates their extrapolation at an industrial level. In the present investigation, the process of synthesis, characterization, and adsorbent capacity of Cd^{2+} of millimetric alumina spheres coated with HAp is described. In addition to this, obtaining an adsorbent material that is easy to handle and can be used as a candidate in adsorption processes at the industrial level was studied.

■ METHODOLOGY

Alumina-HAp Spheres (A-HAp). Alumina spheres were obtained by the ionic encapsulation method previously
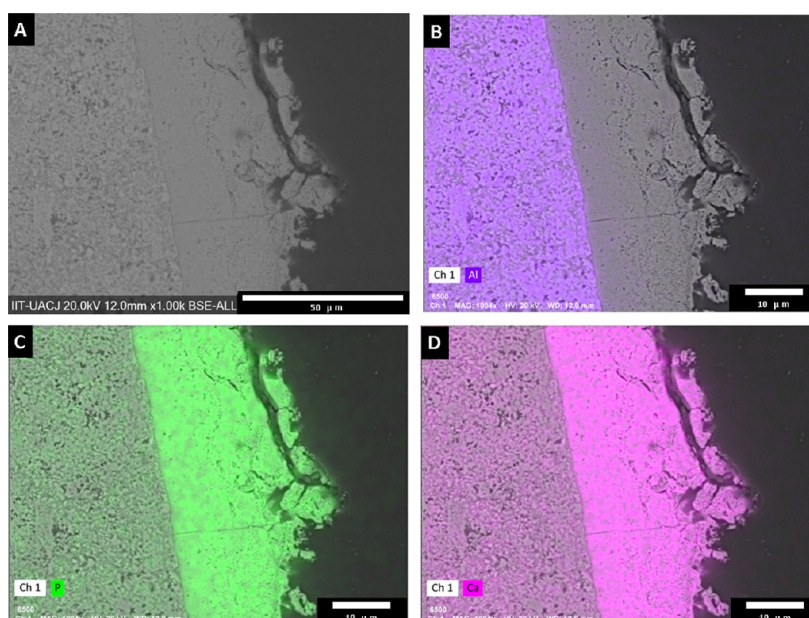
Figure 3. (A) SEM micrographs of the cross section of Al$_2$O$_3$–HAp spheres. Elemental distribution of (B) aluminum, (C) phosphorus, and (D) calcium.
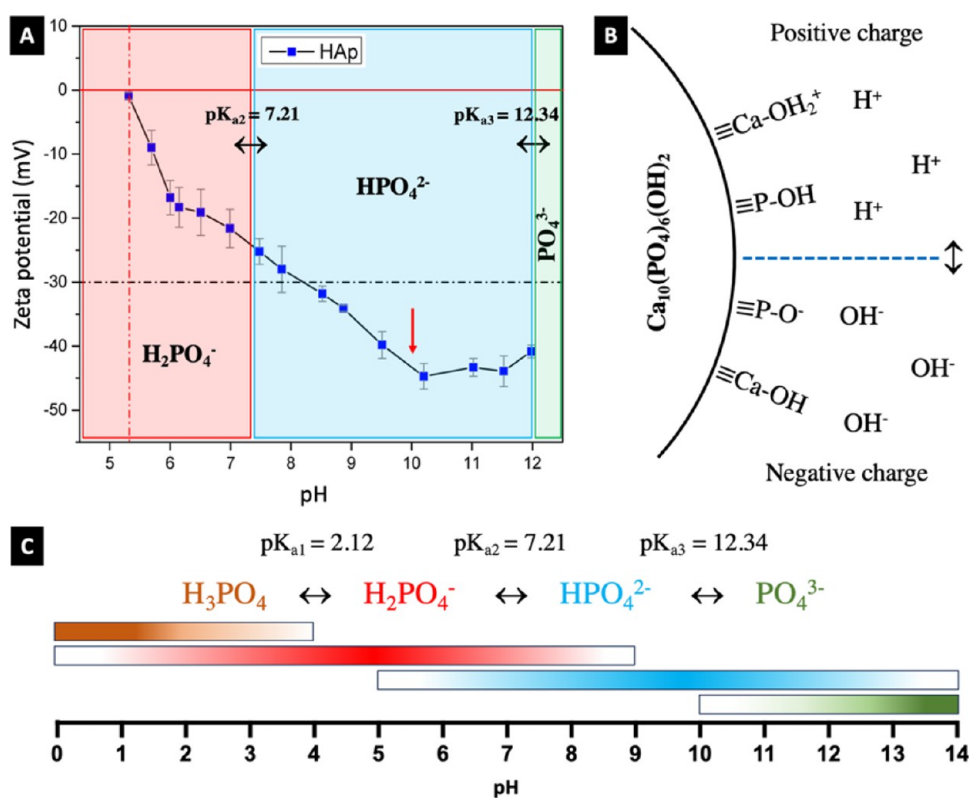

Figure 4. (A) pH vs zeta potential curve of hydroxyapatite treated at 970 °C. (B) Scheme of the hydroxyapatite surface determined by the pH of the medium. (C) Scheme of species distribution of phosphoric acid.

described by Silva-Holguín et al.[13] The synthesis of HAp was carried out by the sol−gel method using calcium nitrate Ca(NO$_3$)$_2$ and triethyl phosphate (P(OCH$_2$CH$_3$)$_3$) as precursors, following the methodology of Garibay-Alvarado et al.[17] To obtain the alumina spheres coated with HAp, the alumina spheres treated at 1600 °C were immersed in the HAp sol−gel, covered with the gel, and allowed to dry at room temperature for 2 h; later, they were subjected to heat treatment at 100 °C for 24 h, followed by 2 h at 400 °C with a heating ramp of 1 °C/min; finally, they were subjected to 970 °C for 2 h with a heating ramp of 5 °C/min.

Characterization. The determined physicochemical properties were textural properties (specific surface area (SSA), pore volume, and pore size), pZ, and active sites (acidic and basic). Textural properties were determined by N$_2$ physisorption using Micromeritics equipment, ASAP 2010 model,
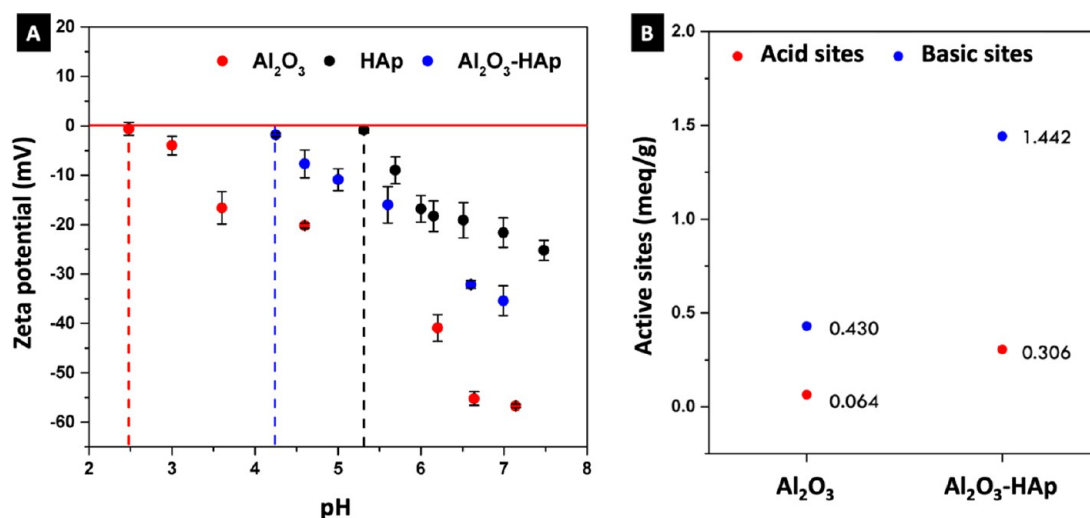
Figure 5. (A) pH vs zeta potential curve of alumina spheres at 1600 °C, hydroxyapatite at 970 °C, and alumina−HAp spheres at 970 °C. (B) Quantification of active sites.
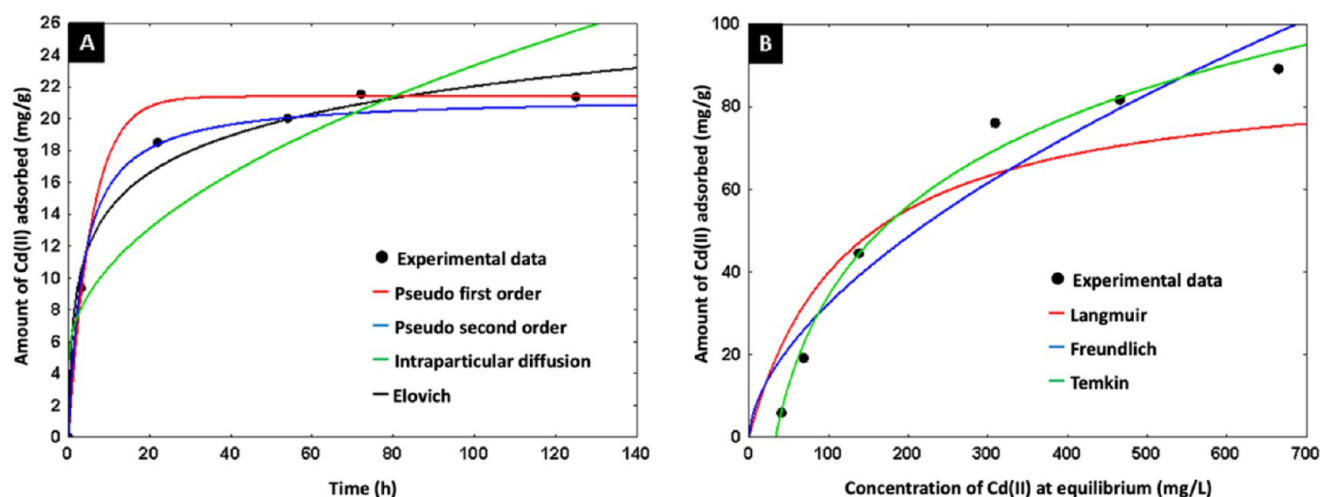

Figure 6. Cd^{2+} adsorption on A-HAp spheres. (A) Adsorption kinetic models. (B) Adsorption equilibrium isotherm.

Table 3. Calculated Kinetic Parameters of Cd (II) Adsorption on Alumina and A-HAp Spheres

		Al$_2$O$_3$	A-HAp
pseudo first order	K_1 (min^{-1})	0.149	0.174
	%D	**4.90**	5.46
	R^2	0.993	0.978
pseudo second order	K_2 (g mg^{-1} h^{-1})	0.015	0.012
	%D	**4.67**	**2.55**
	R^2	0.987	0.995
Elovich	α (mg g^{-1} min)	**30.65**	**51.67**
	β (g mg^{-1})	**0.15**	**0.12**
	%D	8.63	5.66
	R^2	0.965	0.984
intraparticular diffusion	K_D (mg/g/min)	1.47	1.85
	I	3.74	4.83
	%D	12.09	14.67
	R^2	0.784	0.812

and the Brunauer−Emmett−Teller (BET) method. The pZ was determined in a Horiba brand particle analyzer, model SZ-100, at different pH levels. The quantification of the active sites (acidic and basic) was carried out by the acid−base titration method proposed by Boehm (94), using 0.1 N NaOH and HCl titrated solutions.

The material was characterized before and after adsorbing cadmium by infrared spectroscopy (IR), X-ray diffraction (XRD), scanning electron microscopy (SEM), and high-

Table 4. Parameters of Cd (II) Adsorption Isotherms in Alumina and A-HAp Spheres

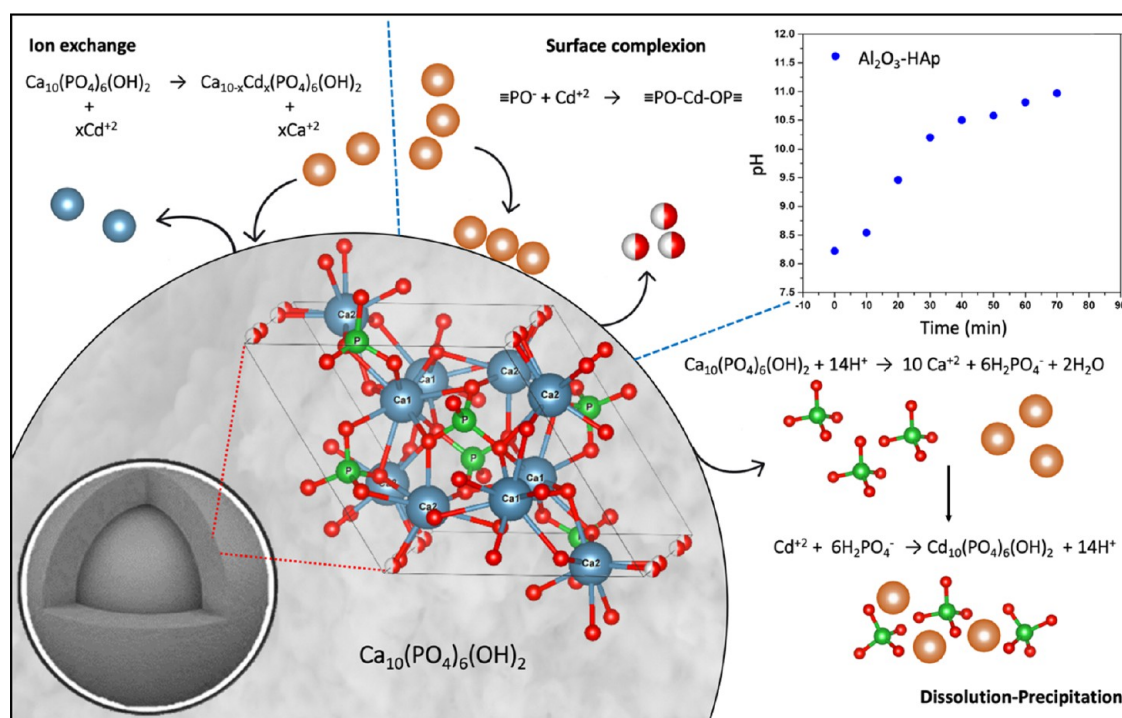|		Al$_2$O$_3$	A-HAp
Langmuir	b (L/mg)	0.0036	0.008
	%D	36.17	23.05
	R^2	0.867	0.854
Freundlich	K_F (mg/g)	0.1404	2.182
	$1/n$	1.092	1.708
	%D	**3.83**	**15.40**
	R^2	0.998	0.916
Temkin	K_T (L/g)	0.0363	0.030
	b	76.13	34.5
	%D	43.75	**6.29**
	R^2	0.836	0.987

Figure 7. Diagram of the mechanism of Cd^{2+} adsorption on alumina−HAp spheres. Inset: change of pH in aqueous solution by alumina−HAp spheres.

resolution transmission electron microscopy (HRTEM). Infrared spectroscopy was carried out using a Bruker Alpha Platinum brand attenuated total reflection (ATR) infrared spectrometer, and 48 scans were performed per powder sample with a range of 4000 to 400 cm^{-1}, with a resolution of 4 cm^{-1}. To determine the crystalline structure of alumina, HAp, and the formation of products derived from cadmium adsorption, the samples were analyzed by the powder diffraction technique in the X'Pert Pro PANalytical instrument, with Cu Kα = 1.54, 20 kV, a 2θ range of 10 to 80°, and a sweep speed of 2°/min. For microstructural analysis, the composites were analyzed in a Hitachi SU5000 field emission SEM with a power of 20 kV and elemental mappings were performed by energy-dispersive X-ray spectroscopy (EDS). For the analysis in the HRTEM brand JEOL JEM 2200FS+CS, the coating of the A-HAp-Cd sphere was scraped ant the detached coating was what was analyzed.

Adsorption Kinetics of Cadmium on Spheres A-HAp. The adsorbent capacity of Cd^{2+} on the alumina-HAp spheres was determined by kinetic and equilibrium adsorption studies. A solution of 1000 mg/g of Cd^{2+} was started using tetrahydrate cadmium nitrate (Cd(NO$_3$)$_2$·4H$_2$O), from which dilutions were made with pH 5 buffer solution of HNO$_3$ and NaOH. The kinetic studies were carried out with 100 mL of Cd^{2+} solution at 200 mg/L, and four spheres were used as adsorbent; the pH was kept constant at 5 with the addition of 0.1 M HNO$_3$. The experimental data were adjusted to the pseudo-first-order, pseudo-second-order, Elovich, and intra-particle diffusion kinetic models; the equation and parameters of each model used are in Table 1.

Equilibrium Adsorption of Cadmium on Spheres A-HAp. Equilibrium adsorption studies were performed with 25 mL dilutions of 20, 50, 100, 200, 400, 600, and 800 mg/L of Cd^{2+}, and using one sphere as adsorbent, the time of contact was 3 days at pH 5 and at room temperature. The experimental data were adjusted to the Langmuir, Freundlich, and Temkin isotherm models; the equation and parameters of each model used are shown in Table 2.

The determination of the cadmium concentration was carried out in ion selective equipment (ISE) and a Thermo Scientific brand Dual Star pH/ISE Benchtop electrode for
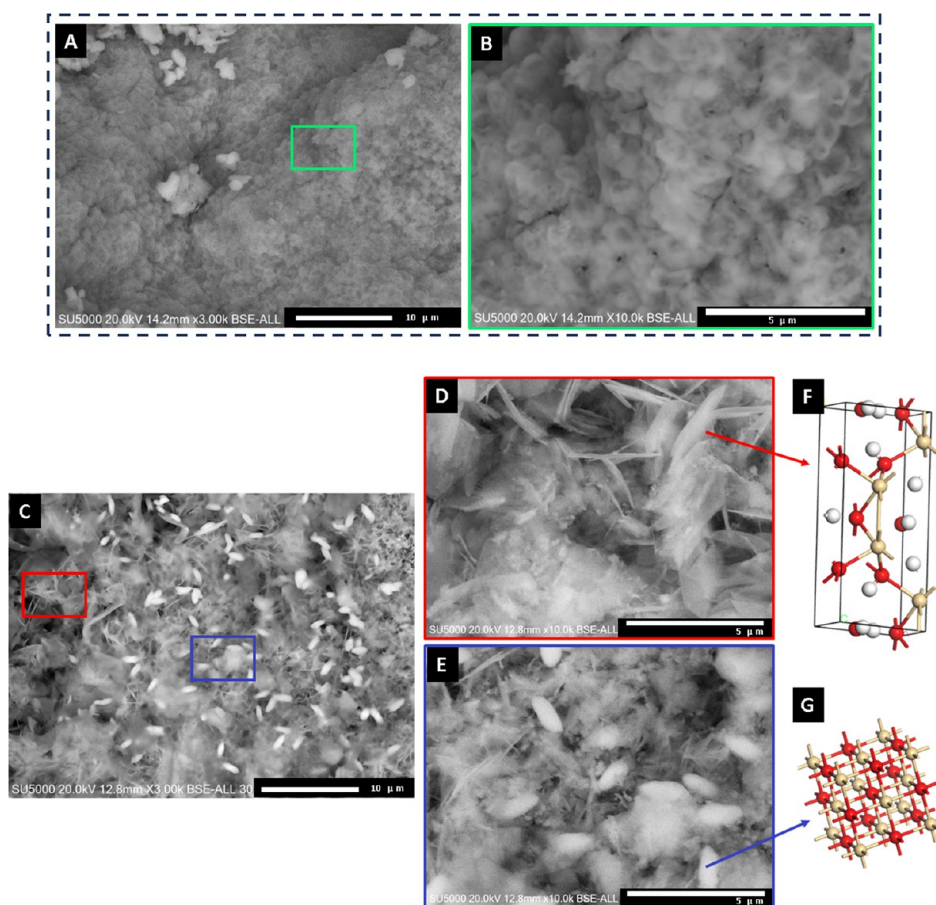
Figure 8. SEM micrographs of spheres surface: (A, B) Al_2O_3–HAp, (C−E) Al_2O_3–HAp-Cd, (F) crystal structure of cadmium hydroxide, and (G) crystal structure of cadmium oxide.

cadmium. The adsorption capacity was determined by means of a mass balance:

$$q = \frac{(V_i{}^*C_i) - (V_f{}^*C_f)}{m}$$

where V_i is the initial volume (L), C_i is the initial concentration (mg/L), V_f is the final volume (L), C_f is the final concentration (mg/L), and m is the mass of the adsorbent (g).

■ RESULTS

The alumina spheres sintered at 1600 °C had a diameter of 4.6 ± 0.3 mm with a weight of 43 ± 2 mg, a specific area of 0.66 m^2/g, a pore volume of 0.0016 cm^3/g, and a pore size of 10. nm. The HAp coating on the alumina sphere of 3.9 ± 0.9 mg corresponded to 8.2% of total sphere weight, and the coating increased the surface area to 0.96 m^2/g, the pore volume to 0.0031 cm^3/g, and the pore size to 13.24 nm, mainly due to the HAp coating.

Figure 1A shows the infrared spectrum of the alumina spheres with a heat treatment at 1600 °C (red), the HAp synthesized by the sol−gel method with heat treatment at 970 °C (black), and the alumina spheres with the HAp coating treated at 970 °C (blue). The spectrum of the alumina sphere shows characteristic bands of α-alumina located at 489, 555, and 631 cm^{-1} corresponding to the AlO_6 octahedral coordination; additionally, a broad and strong absorption is shown in the region from 582 to 937 cm^{-1} corresponding to AlO_4 tetrahedral coordination indicating the formation of a spinel-like β-alumina.[13] The HAp spectrum shows bands at 560, 600, 628, 961, 1022, and 1090 cm^{-1} corresponding to the phosphate group $(PO_4{}^{-3})$.[17,18] The infrared spectrum of the alumina sphere with HAp shows the described bands of alumina with the addition of two bands located at 1022 and 1090 cm^{-1} corresponding to the phosphate group. The reduced intensity in the phosphate group bands indicates a low proportion of HAp in the coating relative to the alumina base material of the sphere. Figure 1B shows the XRD analysis, where the diffractogram of the alumina sphere treated at 1600 °C (red) shows the presence of α-, β-, and γ-alumina. The HAp diffractogram (black) shows characteristic peaks of HAp with a hexagonal crystalline phase and a $P6_3/m$ space group according to crystallographic card COD no. 96-900-1234. The A-HAp sphere (blue) shows a hybrid of the peaks of the found phases of alumina and HAp, where the HAp peaks present low intensity, and most of them are overshadowed by the alumina peaks. Only the (211), (202), and (222) planes of the HAp could be identified. Performing phase quantification, it was determined that 89% corresponds to alumina (α, β, and γ) and 11% to HAp in the A-HAp sphere. When comparing the results of XRD and IR, no structural change of the alumina phases with HAp or of the HAp coating is observed in obtaining the A-HAp composite.

Figure 2 shows micrographs of the SEM of the alumina spheres with a heat treatment at 1600 °C (A,B) and with the HAp coating treated at 970 °C (C−F). The alumina spheres present two morphologies as shown in Figure 2A,B, one in the form of hexagonal plates corresponding to β-alumina[13] and
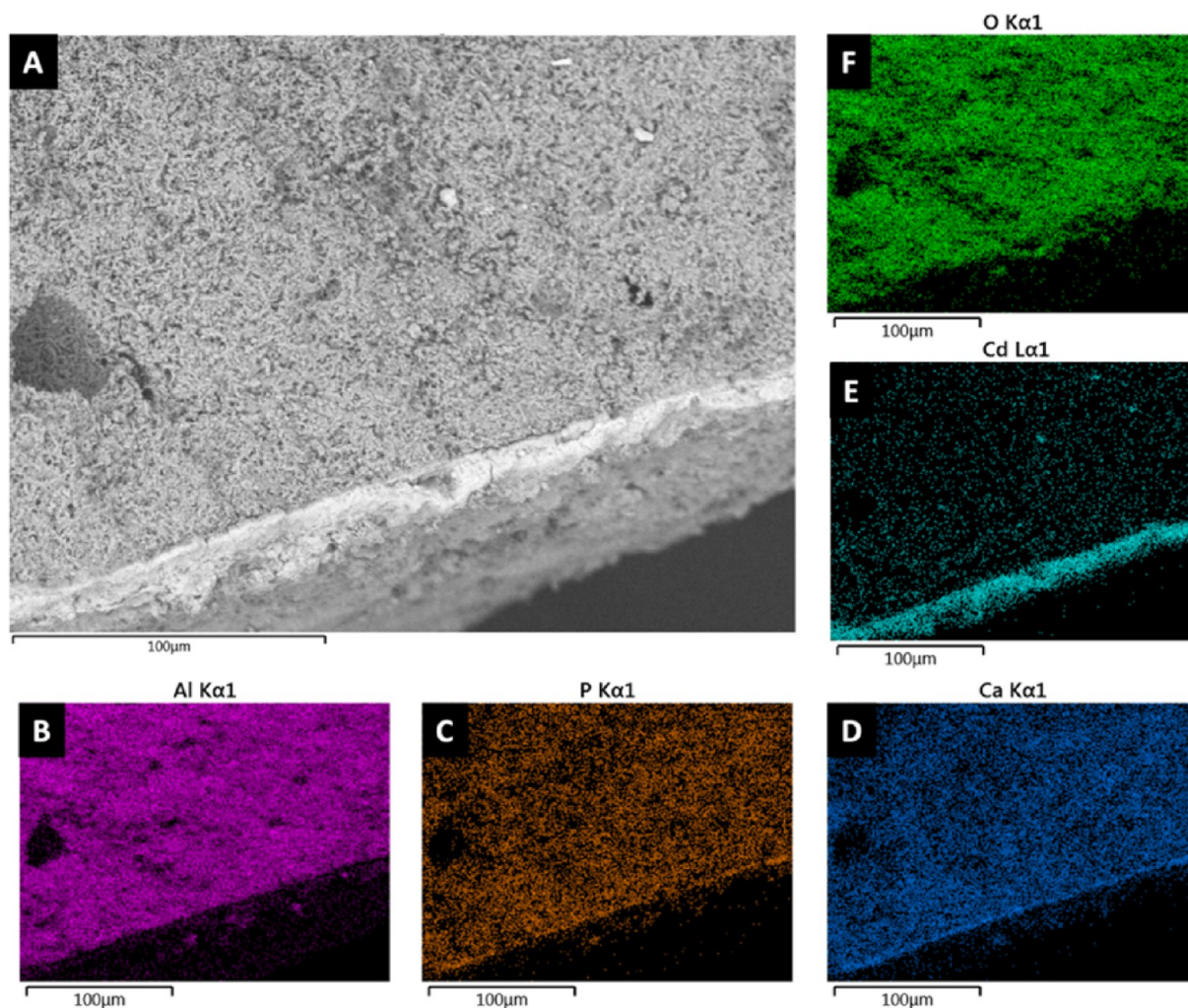
Figure 9. (A) SEM micrograph of the cross section of Al_2O_3−HAp-Cd spheres. Elemental distribution mapping of (B) aluminum, (C) phosphorus, (D) calcium, (E) cadmium, and (F) oxygen.

another in the form of grains corresponding to α-alumina. Figure 2C shows a cross section of the alumina sphere with the HAp coating where two phases of the sphere are clearly observed: the HAp coating (red zone) and the alumina sphere (blue zone). On the surface of the A-HAp sphere, the agglomerated HAp is observed (Figure 2D), while in the alumina sphere, a migration of HAp is observed inside the sphere with the coating of each grain of alumina, as shown in the Figure 2E,F. The elemental distribution mapping by EDS in Figure 3 shows the delimitation of the alumina sphere (Figure 3B), the HAp coating (Figure 3C,D) has a thickness of approximately 30 μm, and calcium and phosphate migration can be seen inside the sphere.

HAp presented an isoelectric point (IEP = ζ_0) at pH 5.37, a pH of maximum stability greater than 8.17, and a maximum pZ of −44.7 ± 2.0, as shown in Figure 4A. The results agree with previous studies indicating an IEP at pH 5.5[19] and a pZ less than −30 mV in deionized water in a range of pH 5.00 to 9.03.[20] The surface charge of HAp is strongly determined by the pH of the medium and the degree of protonation of a specific apatite surface.[21] At acidic pH, the HAp surface is protonated and the positive charge ($\equiv$Ca−OH^{2+}) prevails, while at basic pH, the deprotonation of the HAp surface occurs and the negative charge ($\equiv$P−O$^-$) prevails, as schematized in Figure 4B. As observed in Figure 4A, as the pH of the medium

decreases, the pZ of HAp also decreases, translating into a diminishing in the structural stability of HAp and its consequent dissolution. The decrease in pH causes the protonation of the phosphate group of the HAp, according to the diagram of the distribution of species of phosphoric acid[22] in Figure 4C. At a pH of maximum stability of HAp (>10), we have the species PO_4^{3-}, structural species of HAp. as the pH is lowered, the species PO_4^{3-} is protonated and forms HPO_4^{2-}, which reduces the stability of HAp; at a lower pH, we have the protonation of the species HPO_4^{2-} to $H_2PO_4^-$, which in the HAp structure is not electrically stable because structural neutrality is not maintained, and at pH where the IEP is found (IEP = 5.37), the dominant species is $H_2PO_4^-$ so the solubility of HAp is total due to the loss of electrical stability. The protonation of the HAp favors the breaking of the calcium−oxygen bonds.[23] As a result of the above, the adsorption processes at acidic pH and the main adsorption mechanism are by dissolution−precipitation, as shown in the Scheme of Figure 7.

Figure 5A shows the curve of pH vs pZ of alumina spheres (red), HAp (black), and A-HAp spheres (blue). The alumina sphere presents an IEP at pH 2.5 with an acidic character due to the dehydration of the treated alumina at 1600 °C.[13] By using HAp as a coating on the alumina sphere, we promote a strong interaction between both components by diffusing the
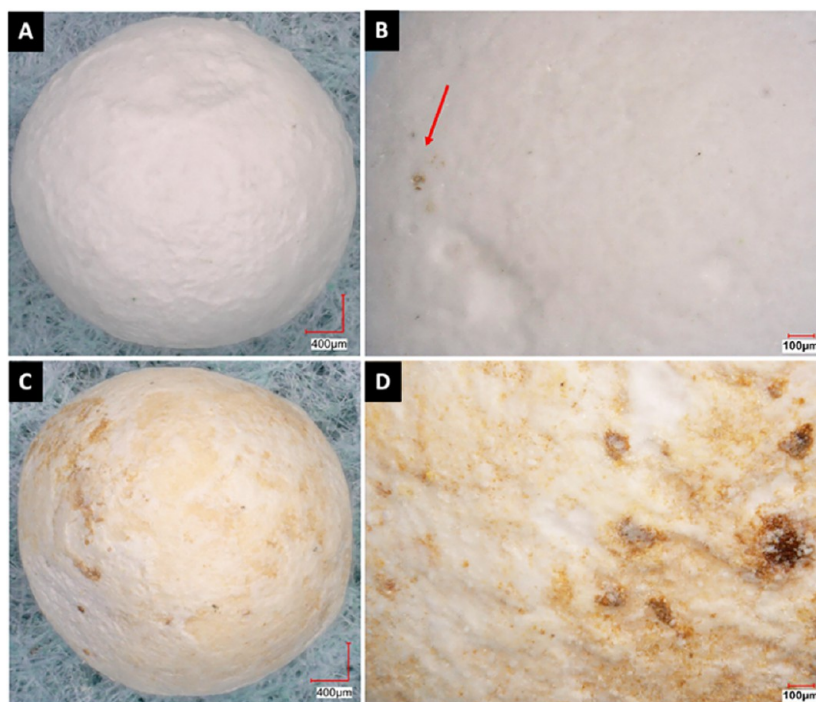
Figure 10. (A, B) Al_2O_3−HAp-Cd spheres and (C, D) Al_2O_3−HAp-Cd spheres with heat treatment at 200 °C.
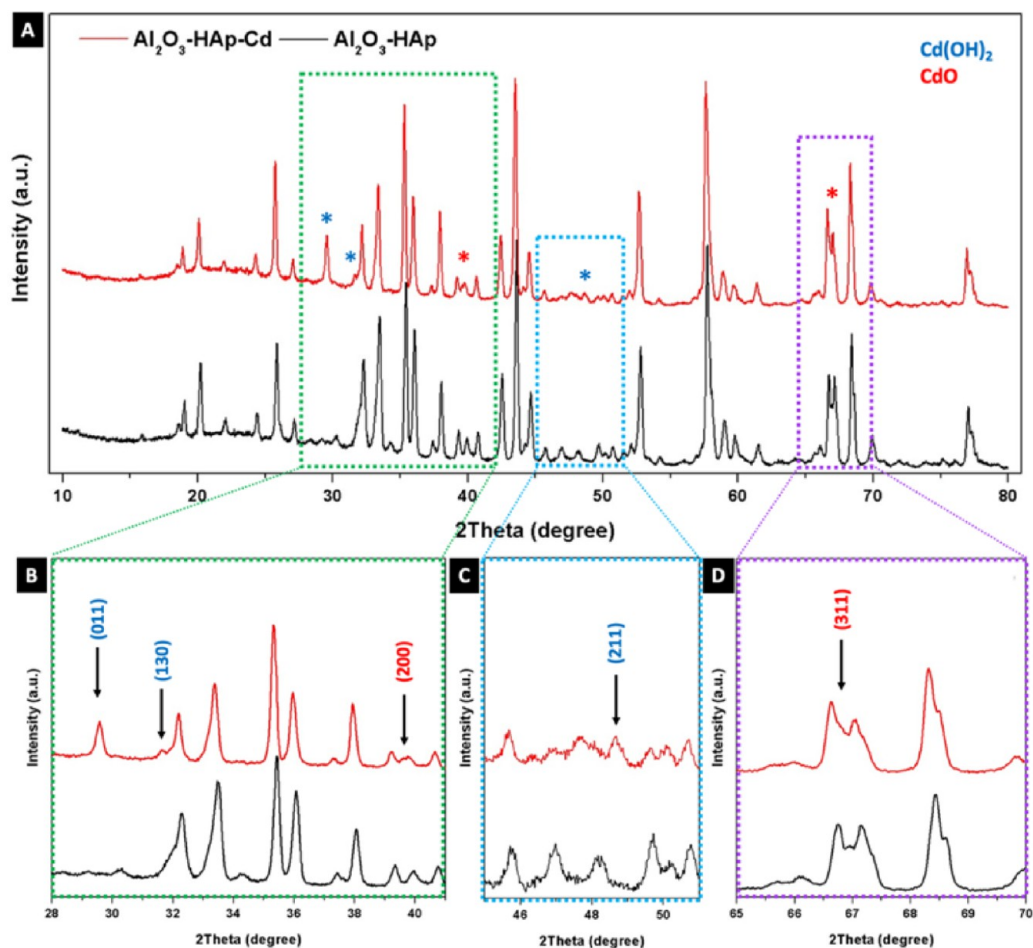

Figure 11. Al_2O_3−HAp spheres after adsorbing cadmium. (A) Al_2O_3−HAp and Al_2O_3−HAp-Cd X-ray diffractogram. (B) Magnification of the green zone. (C) Magnification of the blue zone. (D) Magnification of the purple zone.
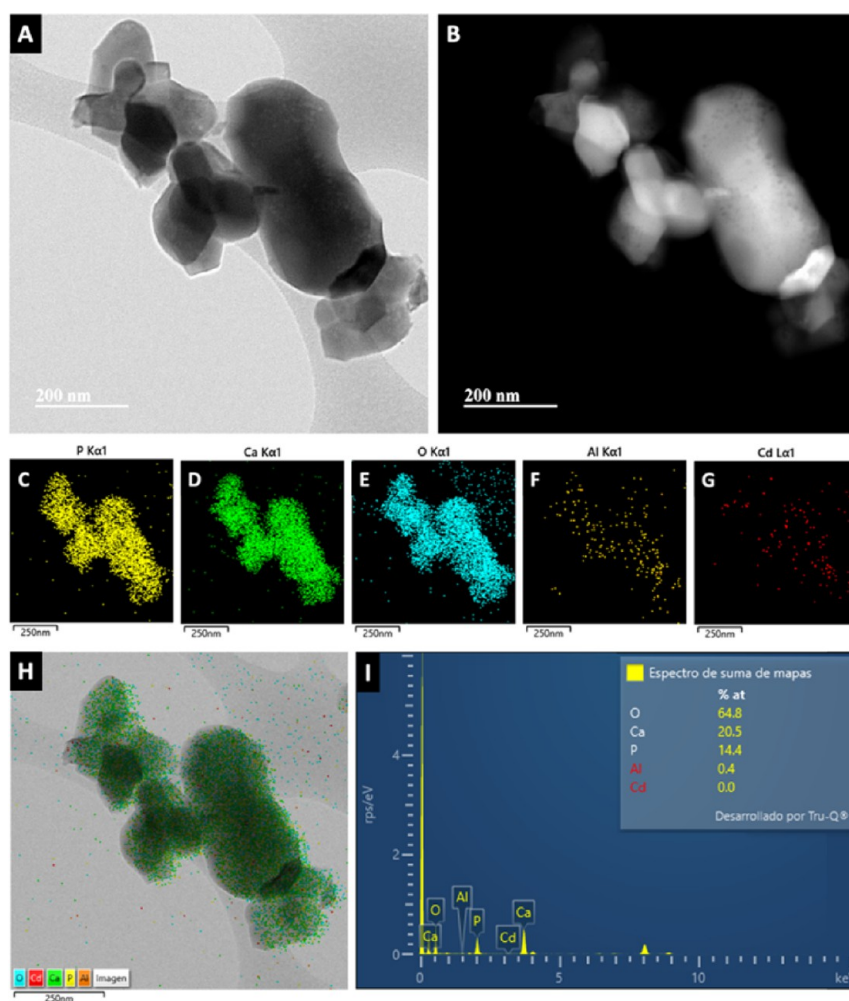
Figure 12. TEM micrographs of A-HAp-Cd HAp particles: (A) bright field and (B) dark field. Elemental distribution of (C) phosphorus, (D) calcium, (E) oxygen, (F) aluminum, and (G) cadmium. (H) Micrograph with elemental distribution. (I) EDS microelement analysis.

HAp into the alumina sphere, shifting the IEP of HAp from 5.37 to 4.2, which increases one unit of pH stability of HAp in alumina compared to pure HAp, so at pH 5 the composite still has a negative charge. The number of acidic and basic active sites was determined on the alumina spheres and with the HAp coating, as shown in Figure 5B. The alumina spheres present 0.064 meq/g of acidic sites and 0.430 meq/g of basic sites. The HAp coating on the alumina spheres increases the number of active sites in the material to 0.306 and 1.442 mequiv/g for the acid and basic sites, respectively. The increase in the negative surface charge and the number of active sites of the composite favors the adsorption process due to electrostatic attractions and the increase in binding sites.

The Cd^{2+} adsorbent capacity of the alumina spheres with the HAp coating was determined by adsorption kinetics and isotherm, as shown in Figure 6. The kinetics in Figure 6A established that 2 days are sufficient for the material to reach an equilibrium. Four kinetic models were applied to describe the Cd^{2+} adsorption mechanism on the A-HAp spheres; the calculated kinetic parameters are shown in Table 3. According to the criterion of least percentage deviation, the pseudo-second-order model best describes the data obtained. The pseudo-second-order model describes the adsorption reaction rate with energetically heterogeneous sites, considering a chemisorption model.[24] In the kinetic parameters of the

Elovich model, an increase in the adsorption rate constant (α) is observed when the alumina sphere is coated with HAp, which indicates that the adsorption process is favored by the HAp coating. On the contrary, the desorption constant (β) has very low values, which indicates that there is little or no desorption. Figure 6B shows the adsorption isotherm where three models were applied to describe the adsorption of Cd^{2+} in the A-HAp spheres; the parameters obtained are shown in Table 4. The models with the lowest percentage of deviation were the Freundlich and Temkin models. The Freundlich model describes a reversible adsorption with the formation of multilayers on a heterogeneous surface, and a value of $1/n$ greater than 1 indicates a cooperative adsorption.[25] Coating the alumina sphere with HAp increases cooperative adsorption on the material, as shown in Table 4. The Temkin model describes adsorption with a uniform binding energy distribution and assumes that the heat of adsorption of all molecules in the adsorption layer decreases linearly with the coating due to adsorbent−adsorbate interactions.[24,26] The maximum adsorption capacity of Cd^{2+} on the alumina spheres was 59.97 mg/g, which was dominated by electrostatic interactions, covalent bonds, and cooperative adsorption, as described in a previous work.[13] The Cd adsorbent capacity increased 1.62 times with the hydroxyapatite coating, obtaining a maximum adsorption of 89.37 mg/g with a respective adsorption of 158 ppm of
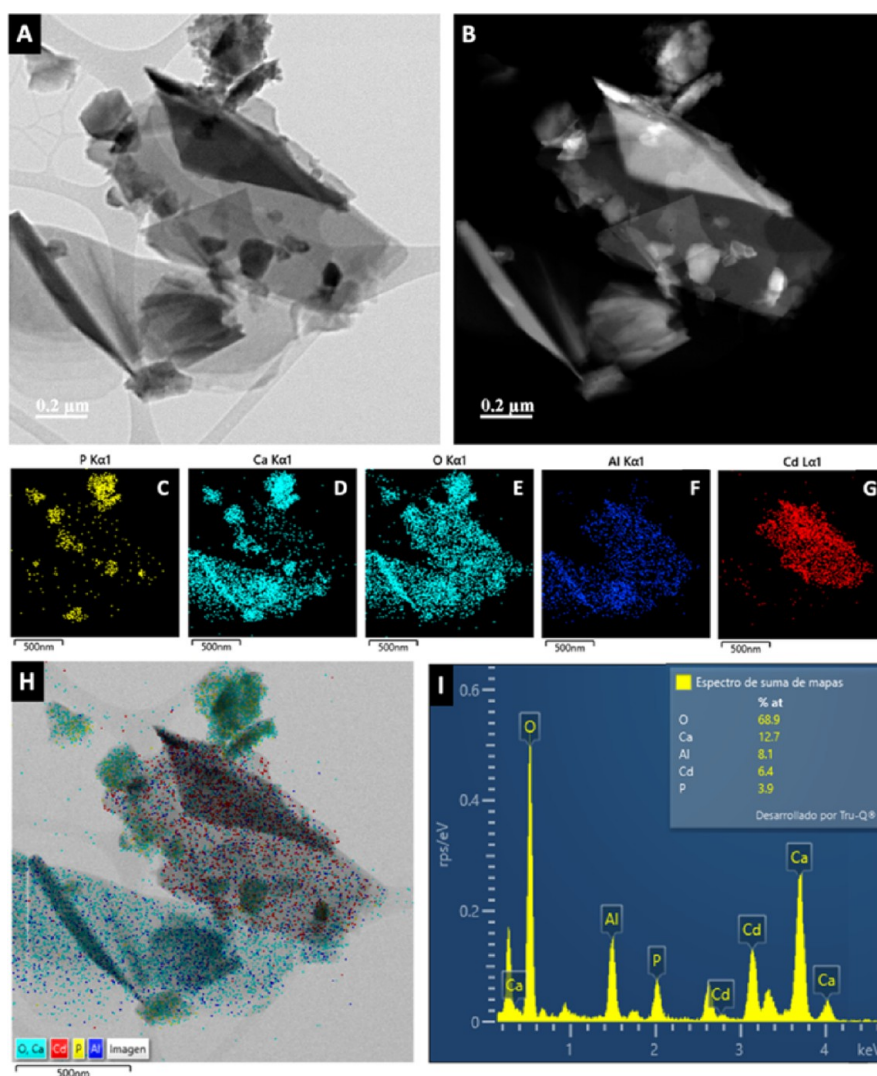
Figure 13. TEM micrographs of A-HAp-Cd particles: (A) bright field and (B) dark field. Elemental distribution of (C) phosphorus, (D) calcium, (E) oxygen, (F) aluminum, and (G) cadmium. (H) Micrograph with elemental distribution. (I) EDS microelement analysis.
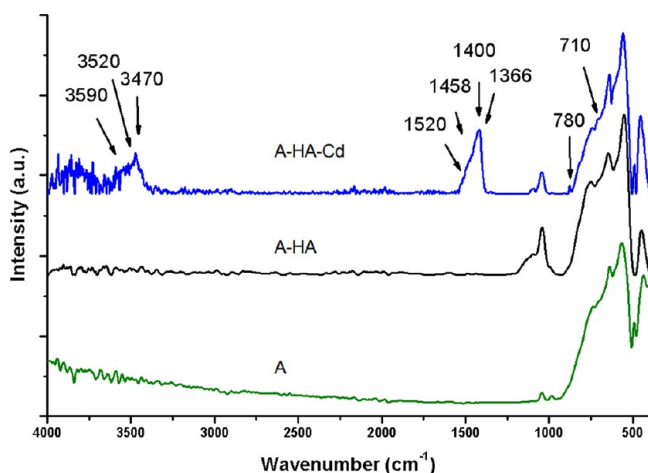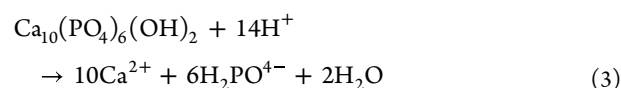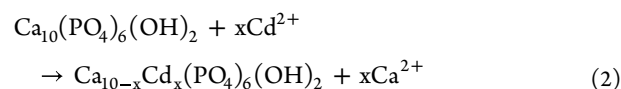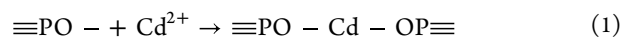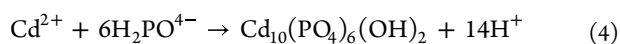

Figure 14. Infrared spectra of the A-HAp-Cd spheres.

Cd^{2+}. According to the fit to the kinetic models and adsorption isotherms, the adsorption of Cd^{2+} on the A-HAp spheres is dominated by chemical interactions where the acid sites of the hydroxyapatite can establish bonds with the Cd^{2+}, and when it

reaches the adsorption equilibrium, a cooperative adsorption occurs where the adsorbate molecules form multilayers causing the accumulation of cadmium on the surface of the material.

The hydroxyapatite adsorption mechanism can occur in three ways: (1) superficial complexation in which the formation of complexes occurs on the surface between the phosphate group (acid site) and Cd^{2+}; (2) ionic exchange between Ca^{2+} in the structure of hydroxyapatite by Cd^{2+}—ionic exchange is favored in alkaline media; (3) dissolution—precipitation—in acidic media, hydroxyapatite is solubilized causing the complexation of phosphate ions and Cd^{2+}, which precipitate in the form of metal phosphate crystals,[27,28] as shown in the scheme of Figure 7; the following reactions display the chemistry involved in the process.

$$\equiv PO - + Cd^{2+} \rightarrow \equiv PO - Cd - OP \equiv \tag{1}$$

$$Ca_{10}(PO_4)_6(OH)_2 + xCd^{2+}$$
$$\rightarrow Ca_{10-x}Cd_x(PO_4)_6(OH)_2 + xCa^{2+} \tag{2}$$

$$Ca_{10}(PO_4)_6(OH)_2 + 14H^+$$
$$\rightarrow 10Ca^{2+} + 6H_2PO_4^{4-} + 2H_2O \tag{3}$$

$$Cd^{2+} + 6H_2PO^{4-} \rightarrow Cd_{10}(PO_4)_6(OH)_2 + 14H^+ \quad (4)$$

The synthesized HAp has an IEP at pH of 5.37, so at pH 5, the HAp is solubilized and cadmium adsorbed by the dissolution−precipitation mechanism; however, when coating the alumina sphere with the HAp, the HAp diffuses inside the alumina sphere, inducing a strong interaction between both components, causing a displacement of the IEP at pH 4.2, which decreases the dissolution of HAp at pH 5 and, therefore, by preventing the dissolution of hydroxyapatite, represses adsorption by dissolution−precipitation and promotes Cd^{2+} adsorption by other mechanisms such as ion exchange and surface complexation. The A-HAp composite in aqueous medium tends to increase the pH of the solution due to the adsorption of H^+ on the hydroxyapatite, as shown in Figure 7A; adjustments in the pH of the solution to pH 5 do not decrease the basic interaction of the hydroxyapatite. The surrounding medium tends to maintain a basic pH, which favors the ion exchange process between Ca^{2+} for Cd^{2+} and/or the formation of cadmium structures on the A-HAp sphere (surface complexation).

Figure 8 shows SEM micrographs of the surfaces of A-HAp spheres before and after adsorbing cadmium. The surface of the A-HAp sphere presents spherical agglomerates of hydroxyapatite, as shown in the SEM micrographs of Figure 8A,B. After the adsorption process, the formation of hierarchical structures like scales (Figure 8D) and denser clusters (Figure 8E) was observed on the entire surface of the sphere, which confirms the adsorption by surface complexation where the formation of cadmium structures occurs on the surface of the A-HAp sphere. The presence of scales denotes the formation of cadmium hydroxide, while the presence of denser clumps denotes the formation of cadmium oxide.[29,30]

Figure 9 shows a micrograph of a cross section of the A-HAp-Cd spheres, where the hydroxyapatite coating and the alumina sphere core can be seen. Elemental distribution mapping shows that cadmium occurs over the entire hydroxyapatite coating, as seen in Figure 9E.

Figure 10 shows an optical micrograph of the A-HAp-Cd sphere where a porous white surface is observed with the presence of certain yellow specks, as indicated in the figure with a red arrow. When subjecting the A-HAp-Cd spheres to 200 °C for 2 h, a change in the color of the surface of the sphere from white to yellow with reddish-brown areas denoting the change from $Cd(OH)_2$ to CdO was observed with heat treatment.[31,32]

To confirm the formation of cadmium oxide and hydroxide, an X-ray diffractogram of the A-HAp-Cd spheres was obtained, as shown in Figure 11. In the spheres, when cadmium was adsorbed, the appearance of peaks was observed in the diffractogram located at 29.56, 31.63, and 48.67° corresponding to the (011), (130), and (211) planes of the $Cd(OH)_2$ formation according to JCPDS card no 84-1767,[33] in addition to the peaks located at 39.73 and 66.78° corresponding to the (200) and (311) planes belonging to CdO according to JCPDS card no 05-0640.[34] No peaks were identified for the formation of a metal phosphate derived from adsorption by dissolution−precipitation.

To establish which is the main mechanism of adsorption, we analyzed the hydroxyapatite crystals on the surface of the A-HAp-Cd sphere by TEM, as shown in Figure 12. The presence of cadmium was not found in the HAp crystals. Therefore, it can be mentioned that there is no ionic exchange in the

structure of HAp. Observing another region of the sample, cadmium scales were observed corresponding to the formation of $Cd(OH)_2$, as shown in Figure 13. Observing the mapping distribution of phosphorus and cadmium in Figure 13C and G, respectively, the presence of phosphorus in the cadmium flakes was not observed, so the formation of a cadmium phosphate by the dissolution−precipitation process is ruled out, as the most likely mechanism in the adsorption of cadmium in the A-HAp spheres is superficial complexation.

Figure 14 shows a green spectrum for alumina (A) and the infrared black spectrum of the alumina spheres with hydroxyapatite (A-HA), and these spectra show the characteristic bands of the alumina spheres of α-Al_2O_3/Ba-β-Al_2O_3 with the addition of three bands of lower intensities at 1094, 1036, and 1005 cm^{-1} corresponding to the P−O bonds of the phosphate group in HAp. The lower intensity of the phosphate group bands is related to the 5 wt % percentage of HAp in the alumina sphere. The blue spectrum for alumina spheres with HAp and cadmium (A-HA-Cd) shows the spheres after the adsorption process; the spectrum shows changes in the region of the range of 4000 to 3000 and 1400 to 1300 cm^{-1}, the spectral region at 3400−3700 cm^{-1} is formed by the chemical species containing OH groups, and two principal bands at 3590 and 3520 are assigned to OH groups in phase according to XRD data. The bands at 1458 and 1520 cm^{-1} are attributed to the bonds of $Cd(OH)_2$. The absorption bands observed at 710, 877, and 1366 cm^{-1} are correlated with the CO_3^{2-} vibrations, the band at 1400 cm^{-1} is assigned to CO_3^{2-} ($\nu3$), and the band at 710 cm^{-1} is assigned to CO_3^{2-} ($\nu2$). The formation of cadmium carbonate is possible because the presence of CO_2 in the solution was not eliminated.[35−36,37]

The choice of efficient adsorbents depends on their cost, their large surface area, their pore size distribution, the presence of functional groups, and polarity. Therefore, it is essential to understand the adsorption process. The effect of ionic strength on the surface charge of the alumina−hydroapatite material was determined by adding 10 mM NaCl. Figure 15 shows the pZ vs pH curve of the A-HAp material in deionized water and a 10 mM NaCl solution; the ionic strength does not induce an effect on the surface charge of the material at acidic pH 4 to 5.5. However, at basic pH,
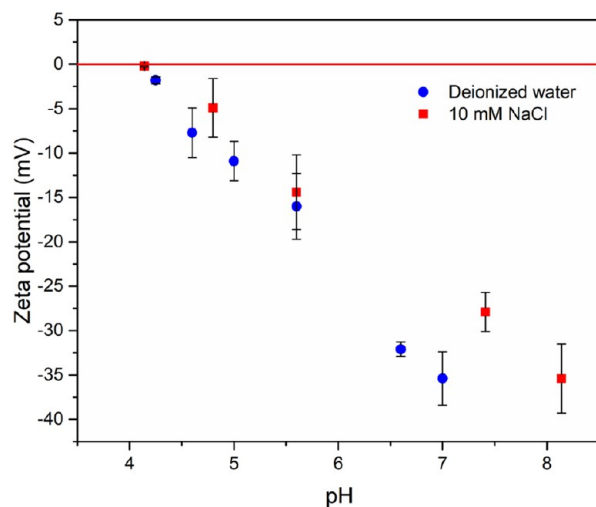

Figure 15. Effect of pH and ionic strength on the measured zeta potential using a sodium chloride.

there is a decrease in the negativity of the material due to the reduction of the diffuse double layer resulting from the ionic strength, leading to an increase in the interaction of the particles.[38] Therefore, cadmium(II) ions will be more effectively removed from chloride solutions according to the literature.[39]

The manuscript shows the preliminary studies of the modification of alumina spheres with hydroxyapatite at the laboratory level with standard solutions of cadmium(II) ions, but according to the results, the material presents adsorbing properties increased by 1.6, which makes the composite a viable and low-cost proposal in aqueous systems for removing cadmium ions because the fragility of the conventionally used hydroxyapatite is improved by being supported and covering a dense spherical alumina ceramic that is easy to handle.

CONCLUSIONS

Alumina–hydroxyapatite spheres show improved adsorbent properties for a potential alternative ceramic adsorption material. The alumina and alumina–hydroxyapatite spheres of ~5 mm were sintered; HAp coating improved the surface area and pore size to 0.96 m^2/g and 13.24 nm and increased the number of acid sites from 0.064 to 0.306 meq/g. The adsorption of Cd^{2+} on the A-HAp spheres is dominated by chemical interactions where the acid sites of the hydroxyapatite with the Cd^{2+} at equilibrium form multilayers of cadmium on the surface of the material. The hydroxyapatite in an insoluble matrix allow surface for complexation instead of adsorption by dissolution precipitation. This is beneficial in adsorption processes at an industrial level because it avoids the use of additional techniques for the recovery of precipitates.

AUTHOR INFORMATION

Corresponding Author

Simón Yobanny Reyes-López − *Laboratorio de Materiales Híbridos Nanoestructurados, Departamento de Ciencias Químico-Biológicas, Instituto de Ciencias Biomédicas, Universidad Autónoma de Ciudad Juárez, Ciudad Juárez 32300, Mexico;* ⊙ orcid.org/0000-0002-9017-3233; Phone: +52-656-688-2100; Email: simon.reyes@uacj.mx

Authors

Pamela Nair Silva-Holguín − *Laboratorio de Materiales Híbridos Nanoestructurados, Departamento de Ciencias Químico-Biológicas, Instituto de Ciencias Biomédicas, Universidad Autónoma de Ciudad Juárez, Ciudad Juárez 32300, Mexico*

Nahum A. Medellín-Castillo − *Multidisciplinary Graduate Program in Environmental Sciences, Autonomous University of San Luis Potosi, 78210 San Luis Potosi, Mexico; Faculty of Engineering, Graduate Studies and Research Center, Autonomous University of San Luis Potosi, 78290 San Luis Potosi, Mexico*

E. Armando Zaragoza-Contreras − *Centro de Investigación en Materiales Avanzados SC, Chihuahua 31136, Mexico;* ⊙ orcid.org/0000-0003-3010-556X

Complete contact information is available at:
https://pubs.acs.org/10.1021/acsomega.3c05418

Author Contributions

REFERENCES

(1) Ain, Q. U.; Zhang, H.; Yaseen, M.; Rasheed, U.; Liu, K.; Subhan, S.; Tong, Z. Facile fabrication of hydroxyapatite-magnetite-bentonite composite for efficient adsorption of Pb (II), Cd (II), and crystal violet from aqueous solution. *Journal of Cleaner Production* **2020**, *247*, 1088.

(2) Bazzi, W.; Abou Fayad, A. G.; Nasser, A.; Haraoui, L. P.; Dewachi, O.; Abou-Sitta, G.; Matar, G. M. Heavy metal toxicity in armed conflicts potentiates AMR in A. baumannii by selecting for antibiotic and heavy metal co-resistance mechanisms. *Frontiers in microbiology* **2020**, *11*, 68.

(3) Baker-Austin, C.; Wright, M. S.; Stepanauskas, R.; McArthur, J. V. Co-selection of antibiotic and metal resistance. *Trends in microbiology* **2006**, *14* (4), 176−182.

(4) Rodgers, K.; McLellan, I; Peshkur, T.; Williams, R.; Tonner, R.; Hursthouse, A. S.; Henriquez, F. L. Can the legacy of industrial pollution influence antimicrobial resistance in estuarine sediments. *Environ. Chem. Lett.* **2019**, *17* (2), 595−607.

(5) Willyard, C. The drug-resistant bacteria that pose the greatest health threats. *Nature News* **2017**, *543* (7643), 15.

(6) Manyangadze, M.; Chikuruwo, N. H. M.; Chakra, C. S.; Narsaiah, T. B.; Radhakumari, M.; Danha, G. Enhancing adsorption capacity of nano-adsorbents via surface modification: A review. *South African Journal of Chemical Engineering* **2020**, *31* (1), 25−32.

(7) Pai, S.; Kini, S. M.; Selvaraj, R.; Pugazhendhi, A. A review on the synthesis of hydroxyapatite, its composites and adsorptive removal of pollutants from wastewater. *J. Water Proc. Eng.* **2020**, *38*, No. 101574.

(8) Pathirana, C.; Ziyath, A. M.; Jinadasa, K. B. S. N.; Egodawatta, P.; Sarina, S.; Goonetilleke, A. Quantifying the influence of surface physico-chemical properties of biosorbents on heavy metal adsorption. *Chemosphere* **2019**, *234*, 488−495.

(9) Mercante, L. A.; Andre, R. S.; Schneider, R.; Mattoso, L. H.; Correa, D. S. Free-standing SiO2/TiO2−MoS2 composite nano-fibrous membranes as nanoadsorbents for efficient Pb (ii) removal. *New J. Chem.* **2020**, *44* (30), 13030−13035.

(10) Vargas-Martínez, N.; Ruíz-Baltazar, Á. D. J.; Medellín-Castillo, N. A.; ReyesLópez, S. Y. Synthesis of α-alumina nano-onions by thermal decomposition of aluminum formate. *J. Nanomater.* **2018**, *2018*, 9061378 DOI: 10.1155/2018/9061378.

(11) Naiya, T. K.; Bhattacharya, A. K.; Das, S. K. Adsorption of Cd (II) and Pb (II) from aqueous solutions on activated alumina. *J. Colloid Interface Sci.* **2009**, *3* (1), 14−26.

(12) Liang, J.; Liu, J.; Yuan, X.; Dong, H.; Zeng, G.; Wu, H.; He, Y. Facile synthesis of alumina-decorated multi-walled carbon nanotubes for simultaneous adsorption of cadmium ion and trichloroethylene. *Chem. Eng. J.* **2015**, *273*, 101−110.

(13) Silva-Holguín, P. N.; Ruíz-Baltazar, Á. D. J.; Medellín-Castillo, N. A.; Labrada-Delgado, G. J.; Reyes-López, S. Y. Synthesis and Characterization of α-Al$_2$O$_3$/Ba-β-Al$_2$O$_3$ Spheres for Cadmium Ions Removal from Aqueous Solutions. *Materials* **2022**, *15*, 6809.

(14) Priyadarsini, S.; Mukherjee, S.; Mishra, M. Nanoparticles used in dentistry: A review. *J. Oral Biol. Craniofacial Res.* **2018**, *8* (1), 40−43.

(15) Sadat-Shojai, M.; Khorasani, M. T.; Dinpanah-Khoshdargi, E.; Jamshidi, A. Synthesis methods for nanosized hydroxyapatite with diverse structures. *Acta biomaterialia* **2013**, *9* (8), 7591−7621.

(16) Zhou, C.; Wang, X.; Wang, Y.; Song, X.; Fang, D.; Ge, S. The sorption of single-and multi-heavy metals in aqueous solution using enhanced nanohydroxyapatite assisted with ultrasonic. *Journal of Environmental Chemical Engineering* **2021**, *9* (3), No. 105240.

(17) Garibay-Alvarado, J. A.; Espinosa-Cristóbal, L. F.; Reyes-López, S. Y.; Garibay-Alvarado, J. A.; Espinosa Cristóbal, L. F.; Reyes-López, S. Y. (2017). *Fibrous silica-hydroxyapatite composite by electrospinning*. Producto de investigación ICB.

(18) Roque-Ruiz, J. H.; Garibay-Alvarado, J. A.; Medellín-Castillo, N. A.; Reyes-López, S. Y. Preparation of electrospun hydroxyapatite-glass fibers for removal of cadmium (Cd^{+2}) and lead (Pb^{+2}) from aqueous media. *Water, Air, Soil Pollut.* **2020**, *231*, 1−13.

(19) Botelho, C. M.; Lopes, M. A.; Gibson, I. R.; Best, S. M.; Santos, J. D. Structural analysis of Si-substituted hydroxyapatite: zeta potential and X-ray photoelectron spectroscopy. *J. Mater. Sci.: Mater. Med.* **2002**, *13* (12), 1123−1127.

(20) Ma, K.; Cui, H.; Zhou, A.; Wu, H.; Dong, X.; Zu, F.; Xu, Q. Mesoporous hydroxyapatite: Synthesis in molecular self-assembly and adsorption properties. *Microporous Mesoporous Mater.* **2021**, No. 111164.

(21) Wu, L.; Forsling, W.; Schindler, P. W. Surface complexation of calcium minerals in aqueous solution: 1. Surface protonation at fluorapatite—water interfaces. *J. Colloid Interface Sci.* **1991**, *147* (1), 178−185.

(22) Rybalkina, O.; Tsygurina, K.; Melnikova, E.; Mareev, S.; Moroz, I.; Nikonenko, V.; Pismenskaya, N. Partial fluxes of phosphoric acid anions through anion-exchange membranes in the course of NaH2PO4 solution electrodialysis. *International Journal of Molecular Sciences* **2019**, *20* (14), 3593.

(23) Kwon, K. Y.; Wang, E.; Chung, A.; Chang, N.; Lee, S. W. Effect of salinity on hydroxyapatite dissolution studied by atomic force microscopy. *J. Phys. Chem. C* **2009**, *113* (9), 69−72.

(24) Mercado-Borrayo, B. M.; Schouwenaars, R.; Litter, M. I.; Montoya-Bautista, C. V.; Ramírez-Zamora, R. M. (2014). Metal-lurgical slag as an efficient and economical adsorbent of arsenic. In *Water reclamation and sustainability* (pp 95−114). Elsevier.

(25) Sahoo, T. R.; Prelot, B. (2020). Adsorption processes for the removal of contaminants from wastewater: the perspective role of nanomaterials and nanotechnology. In *Nanomaterials for the detection and removal of wastewater pollutants* (pp 161−222). Elsevier.

(26) Al-Ghouti, M. A.; Da'ana, D. A. Guidelines for the use and interpretation of adsorption isotherm models: A review. *Journal of hazardous materials* **2020**, *393*, No. 122383.

(27) Ibrahim, M.; Labaki, M.; Giraudon, J. M.; Lamonier, J. F. Hydroxyapatite, a multifunctional material for air, water and soil pollution control: A review. *Journal of hazardous materials* **2020**, *383*, No. 121139.

(28) Zhou, C.; Wang, X.; Song, X.; Wang, Y.; Fang, D.; Ge, S.; Zhang, R. Insights into dynamic adsorption of lead by nano-hydroxyapatite prepared with two-stage ultrasound. *Chemosphere* **2020**, *253*, No. 126661.

(29) Prammitha, R.; Samson, Y.; Jeice, R. Synthesis of Cd (OH) 2-CdO Nanoparticles Using Veldt Grape Leaf Extract: Enhanced Dye Degradation and Microbial Resistance. 2022.

(30) Selvam, N. C. S.; Kumar, R. T.; Yogeenth, K.; Kennedy, L. J.; Sekaran, G.; Vijaya, J. J. Simple and rapid synthesis of cadmium oxide (CdO) nanospheres by a microwave-assisted combustion method. *Powder technology* **2011**, *211* (2−3), 250−255.

(31) Ullah, H.; Rahaman, R.; Mahmud, S. Optical properties of cadmium oxide (CdO) thin films. *Indonesian Journal of Electrical Engineering and Computer Science* **2017**, *5* (1), 81−84.

(32) Prakash, T.; Arunkumar, T.; Raj, D. S.; Jayaprakash, R. Surfactant-liaised variation in CdO nanocomposites morphology. *Phys. Procedia* **2013**, *49*, 36−43.

(33) Mirzaei, A.; Jamshidi, E.; Morshedloo, E.; Javanshir, S.; Manteghi, F. Carrageenan assisted synthesis of morphological diversity of CdO and Cd (OH) 2 with high antibacterial activity. *Materials Research Express* **2021**, *8* (6), No. 065006.

(34) Kumar, S.; Ahmed, B.; Ojha, A. K.; Das, J.; Kumar, A. Facile synthesis of CdO nanorods and exploiting its properties towards supercapacitor electrode materials and low power UV irradiation driven photocatalysis against methylene blue dye. *Mater. Res. Bull.* **2017**, *90*, 224−231.

(35) Bucca, M.; Dietzel, M.; Tang, J.; Leis, A.; Köhler, S. J. Nucleation and crystallization of otavite, witherite, calcite, strontian-ite, hydrozincite, and hydrocerussite by CO2 membrane diffusion technique. *Chem. Geol.* **2009**, *266*, 143−156.

(36) Hernández-Borja, J.; Ramírez-Bon, R.; Vorobiev, Y. V.; Hernández-Landaverde, M. A. Chemically deposited ammonia-free cadmium hydroxide thin films. *Thin Solid Films* **2016**, *615*, 256−260.

(37) Mazaheritehrani, M.; Asghari, J.; Lotfi Orimi, R.; Pahlavan, S. Microwave-assisted synthesis of nano-sized cadmium oxide as a new and highly efficient catalyst for solvent free acylation of amines and alcohols. *Asian J. Chem.* **2010**, *22* (4), 2554.

(38) Badawy, A. M. E.; Luxton, T. P.; Silva, R. G.; Scheckel, K. G.; Suidan, M. T.; Tolaymat, T. M. Impact of environmental conditions (pH, ionic strength, and electrolyte type) on the surface charge and aggregation of silver nanoparticles suspensions. *Environ. Sci. Technol.* **2010**, *44* (4), 1260−1266.

(39) Ciesielczyk, F.; Bartczak, P.; Jesionowski, T. A comprehensive study of Cd(II) ions removal utilizing high-surface-area binary Mg—Si hybrid oxide adsorbent. *Int. J. Environ. Sci. Technol.* **2015**, *12*, 3613−3626.